IEEE Access
Multidisciplinary ⋮ Rapid Review ⋮ Open Access Journal

Received 12 February 2024, accepted 11 March 2024, date of publication 4 April 2024, date of current version 19 April 2024.

Digital Object Identifier 10.1109/ACCESS.2024.3384977

RESEARCH ARTICLE

Self-Healing Effects in OAM Beams Observed on a 28 GHz Experimental Link

MAREK KLEMES, (Life Senior, IEEE), LAN HU, GREGORY J. BOWLES, MOHAMMAD AKBARI, (Member, IEEE), SOULIDETH THIRAKOUNE, MICHAEL SCHWARTZMAN, KEVIN ZHANG, TAN HUY HO, DAVID WESSEL, AND WEN TONG, (Fellow, IEEE)

Canada Research Center, Huawei Technologies Canada Company Ltd., Kanata, ON K2K 3J1, Canada

Corresponding author: Marek Klemes (marek.klemes@huawei.com)

This work was supported by Canada Research Center, Huawei Technologies Canada Company Ltd., Kanata, ON, Canada.

ABSTRACT In this paper we document for the first time some of the effects of self-healing, a property of orbital-angular-momentum (OAM) or vortex beams, as observed on a millimeter-wave experimental communications link in an outdoors line-of-sight (LOS) scenario. The OAM beams have a helical phase and polarization structure, and have conical amplitude shape in the far field. The Poynting vectors of the OAM beams also possess helical structures, orthogonal to the corresponding helical phase-fronts. Due to such non-planar structure in the direction orthogonal to the beam axis, OAM beams are a subset of ''structured light'' beams. Such structured beams are known to possess self-healing properties when partially obstructed along their propagation axis, especially in their near fields, resulting in partial reconstruction of their structures at larger distances along their beam axis. This has practical implications in siting antennas where obstructions due to people or vegetation may occur. Various theoretical rationales have been proposed to explain, model and experimentally verify the self-healing physical effects in structured optical beams, using various types of obstructions and experimental techniques. Based on these models, we hypothesize that any self-healing observed will be greater as the OAM order increases. Here we observe the self-healing effects for the first time in structured OAM radio beams, in terms of communication signals and channel parameters rather than beam structures. We capture the effects of partial near-field obstructions of OAM beams of different orders on the communications signals, and provide a physical rationale to substantiate that the self-healing effect was observed to increase with the order of OAM, agreeing with our hypothesis.

INDEX TERMS Self-healing, orbital angular momentum (OAM), millimeter waves, vortex beam, helical phase, helical Poynting vector, partial beam obstruction, structured light, conical beam, Butler matrix, DFT matrix, phase gradient, phase velocities, transverse wave vector, error-vector magnitude (EVM).

I. INTRODUCTION

As the demand for wireless services continues to grow, successive generations of radio transmission technology have evolved to accommodate increasing numbers of users and their volumes of data. Refinements in the exploitation of the familiar time and frequency dimensions of wireless signals have begun to approach the limits of their capacity to deliver the required volumes of data at the rates and qualities of the growing demand, so by the 5-th generation (5G) the spatial dimension was opened to create even more user channels, in the form of multiple-antenna systems collectively known as multi-input multi-output (MIMO), which relied on the scattering environment to form diverse spatial paths from

The associate editor coordinating the review of this manuscript and approving it for publication was Chinmoy Saha.

transmitter to one or more receivers. This included the two possible dimensions of polarization which have been in use for some time as means of increasing the channel capacity of fixed microwave backhaul links as their frequency allocations began to be exhausted.

Work is now well under way on the 6-th generation of wireless technology (6G) as demand for connectivity grows from connected personal users to connected sensors, automobiles and the wireless internet of things (IOT), and along with it, the search for more signal dimensions continues. It has been found that the phase structure of wireless signal waves can be open to more variety beyond that of plane waves, especially at the higher frequencies where antennas occupy less space and their beams are more controllable. Specifically in the field of optics, it has been found some 32 years ago that light can carry orbital angular momentum (OAM), in addition to the well-known spin angular momentum (SAM, also known as polarization) [1].

The OAM manifests as a linear progression of electrical phase of the beam around its axis, completing an integer number, *l,* of 360-degree cycles of phase in one physical 360-degree orbit around the axis of propagation. Its far-field amplitude pattern has a conical shape, as shown in Figure 1. Its phase has a helical pattern, the equi-phase contours forming spirals around the beam axis. In the physics and optics community, OAM was typically effected on laser light by means of a spiral dielectric phase plate whose thickness varied as a linear function of azimuth angle such that the slope of the phase delay was an integer number of degrees per degree of azimuth angle. (It turns out that some quarter-century before that, a similar effect was in use in radio-frequency (RF) circular antenna arrays, but radiating mostly in the azimuth plane, and was known as phase-modes [2].) As there is no theoretical limit to the number of phase cycles around the beam axis, OAM became another signal dimension open to exploitation in 6G wireless technology development. Other structured beams and their properties, already studied in the optics community, have also come into consideration for future wireless applications.

One appealing property of structured beams is that of self-reconstruction, or ''self-healing'' of its structure when it is partially obstructed close to its source aperture [3]. It allows for siting OAM antennas where partial obstructions due to vegetation or people may occur. This sets them apart from other MIMO antenna radiations which rely on a rich scattering environment to effect their spatial diversity, but also incur obstruction losses. Having been characterizing a 28 GHz millimeter-wave OAM multiplexing wireless link as the subject of previous publications [4], it was of interest for us to observe any evidence of self-healing of the OAM beams, from the point of view of the communications link parameters, rather that the physical structures of the beams as has mostly been done in the optical community.

The paper is organized as follows: Section II summarizes the experimental millimeter-wave (mm-wave) link, especially the multi-OAM transmitting antenna and its design rationale. Section III describes the self-healing experiments and summarizes the measured link performance data. Section IV analyzes the measured data and presents a physical rationale to account for the observed results, while section V draws the conclusions and outlines areas for future investigations.

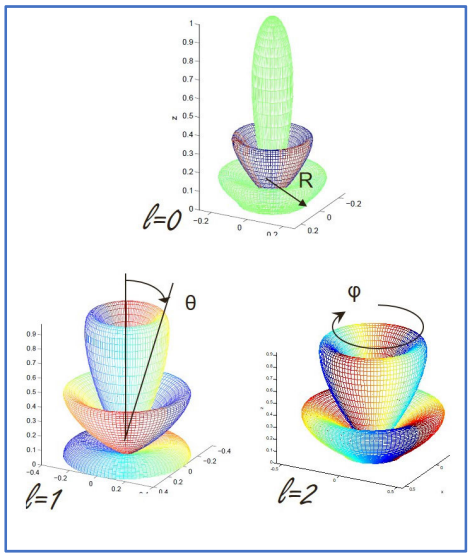

FIGURE 1. Examples of OAM beams of order l = 0, +1, +2 generated by a uniform circular array. Colour denotes electrical phase, amplitude is normalized to peak value and propagation is along z axis (vertical).

II. EXPERIMENTAL OAM OUTDOOR LINK AND OAM ANTENNA DESIGN

The OAM experimental test bench was designed as a one-way line-of-sight (LOS) link with the multi-mode OAM antenna transmitting an independent data stream on each of up to 5 mutually-orthogonal OAM beams to one multi-receiver user equipment (UE) fitted with a linear array of up to 4 antennas and corresponding receivers. More details of the original configuration are contained in reference [4]; some details were re-configured for purposes of the present experiments, as detailed in Table 1. Layout of the link and the equipment at each end is depicted in Figure 2. To keep sizes manageable, the RF was selected as 28 GHz, for a typical link length of 50m, with a far field ranging from 30m to 200m. To minimize perturbations of the OAM beams, the polarization was chosen as right-hand circular polarization (RHCP) at both ends, which would help to reject ground reflections, as all the equipment was mounted on movable carts at less than 2m from the ground. Accordingly, it was desired to keep the radius, *R*, of the conical OAM beams at the receiver to ∼2m, so that the receiving (RX) antenna array could capture a significant portion of the beams, which in turn determined the size of the transmitting (TX) OAM antenna.

Additionally, all of the OAM beams needed to have the same cone radii so that they would overlap at the

TABLE 1. Experimental OAM link and TX antenna parameters.

Parameter	Symbol	Relation	Value	Units
Desired link specification.				
Signal bandwidth	B	(LTE channel)	20	MHz
Number of OAM modes	K	Co-channel data streams	5	1
Link distance	L	TX to RX	50	m
RX antenna separation	d	Max. UE antenna spacing	0.20	m
Digital IF of RX	F	ADC bandwidth	983.04	MHz
Dependent link parameters				
OAM beam radius	R	$R< dF/(2B)$ $R=0.87m$	2.4576	m
RF wavelength	λ	$28.0\text{x}10^9$ $/3.0\text{x}10^8$	0.011	m
TX antenna radius (max).	r	$r\sim(K-1)\lambda L/(4\pi R)$	0.201	m
TX far field	L_{far}	$2(2r)^2/\lambda$	32.35	m
No. of TX array elements (max)	N	$N\sim 2\pi r/(\lambda/2)$	238	1

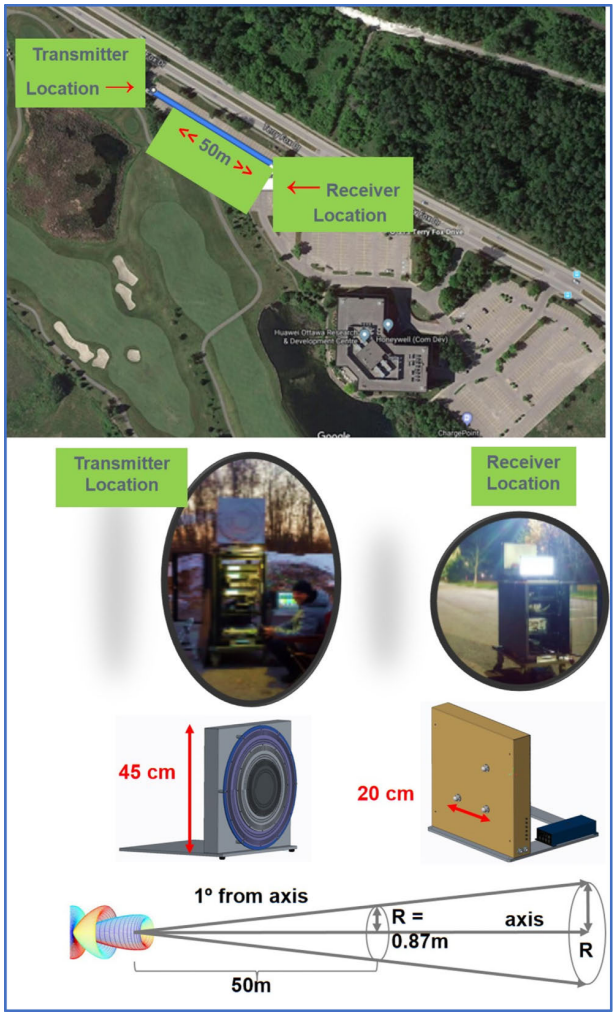

FIGURE 2. Layout of experimental outdoor OAM link and 28 GHz transmitting and receiving equipment.

receiving end, because each beam carried a separate data stream on the same common RF carrier frequency, which

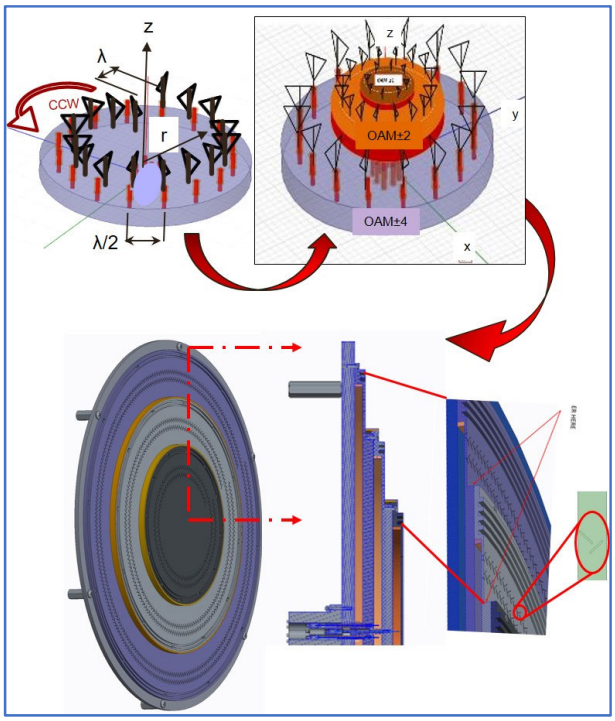

FIGURE 3. Design of multi-mode OAM antenna, showing radially-oriented RHCP array elements, arranged in a clockwise outward spiral to compensate rotation phase of RHCP, stacked in discs of increasing radii for increasing OAM orders, with cross-section detail and detail of RHCP crossed-slots array elements.

needed to be de-multiplexed in the receiver. Therefore the TX antenna was composed of 3 concentric circular-array antennas, with the larger ones transmitting the correspondingly higher orders of OAM beams. Up to 5 OAM beams could be transmitted.

Each array is a type of radial line slot array (RLSA), fed with a small circular array of probes around the center of the radial waveguide. Figure 3 depicts the TX multi-mode OAM antenna design. Its far-field radiation pattern of the ℓ-th OAM mode can be analytically described by the equation

$$F_\ell(\theta,\varphi) = (-j)^\ell e^{j\ell\varphi} K J_\ell\left(\frac{2\pi r \sin\theta}{\lambda}\right) \quad (1)$$

where r is the radius of the transmitting circular (actually spiral) array radiating the ℓ-th OAM mode, λ is the radiating wavelength, J_ℓ is the ℓ-th order Bessel function of the first kind, K is a constant of propagation, θ is the elevation or tilt angle from the beam (z) axis while φ is the azimuth angle around the beam axis as well as the electrical phase of the beam at that azimuth angle in the far field.

The receiving antenna array of 4 horns was positioned at a distance of $L = 50$m from the transmitting OAM antenna, which was tilted upward so as to place the receiver at the bottom arc of the 1° cone of the OAM+2 beam transmitted from the middle RLSA and also the 1° cone of OAM+4 transmitted from the largest RLSA. Up to 4 OAM beams can be received.

The radial profiles of these two OAM beams follow equation (1), each RLSA radius r being designed so that the amplitude patterns of these two OAM beams coincide in the far field with $r_{OAM2} = 0.149$m and $r_{OAM4} = 0.218$m, as illustrated in Figure 4. Note that the diameters of the OAM+2 (green curve and outlined inset), and the scaled OAM+4 (red curve and outlined inset) are now both equal, corresponding to a cone angle of about 1.43 degrees from the beam axis. The receiver array was actually placed somewhat inside these conical beams, at $\theta \sim 1.0°$ because the phase gradients with respect to azimuth angle φ were less rippled there, according to electromagnetic simulations of the OAM antenna. This scaling of the OAM amplitude profiles then leaves their ***azimuth (or circumferential) phase profiles as the main structural difference between the OAM+2 and OAM+4 beams, to which any self-healing may be attributed***.

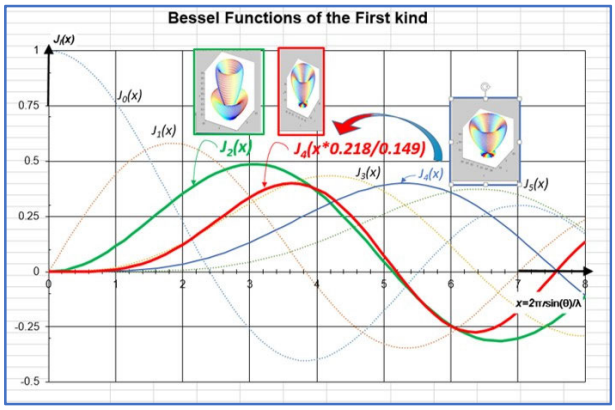

FIGURE 4. Scaling of OAM+4 amplitude profile to make its cone radius the same as cone radius of OAM+2 in the far field. OAM+2 is sourced from aperture of diameter 0.149m (green) so OAM+4 (blue) must be sourced from aperture of diameter 0.218m (red) to overlap with OAM+2 beam at the receiver.

This is very important, because we want to avoid causing similar effects as signs of self-healing, by other effects not related to their phase structuring, such as the differences in angular size of the central nulls and in the peak directivities of the OAM beams. Transmitted signal levels were adjusted to be equal in the OAM+2 and OAM+4 beams at the receiver.

III. EFFECTS OF PARTIAL BEAM OBSTRUCTION AND SELF-HEALING IN OAM+2 AND OAM+4 BEAMS

In order to observe the effects of partial beam obstruction and discern that self-healing is taking place in the OAM beams, only relative measurements could be made, as the experimental link did not possess equipment capable of characterizing the entire beam structures. Specifically, the types of relative measurements of interest pertained to the communications parameters of the LOS link, much like in a MIMO link, such as signal-to-noise ratio (SNR), EVM, and phase gradient among the 4 antennas in the receiving array.

According to findings in recent literature, the self-healing effect in structured EM beams is typically evident in the presence of partial obstructions in their near fields [5], and significantly dependent on the wavelengths, especially in the region of mmm-waves. It is also not complete healing, depending on the relative size and position of the partial obstruction, which makes it difficult to quantify analytically [5], [6]. It is generally evident that structured beams which possess the largest proportions of wave vectors which have different directions from that in the direction of beam propagation (along its optical axis, z), also exhibit the greatest degrees of self-healing and structural robustness [5], [6], [7].

Our hypothesis in these experiments was that OAM+2 will suffer relatively more ''damage'' and phase perturbation than OAM+4 when each is impaired by the same obstruction at the same location in their common near field. That would correspond to the latter beam having greater self-healing ability than the former, lower-order OAM beam. If even partial self-healing does not occur, then our corresponding null hypothesis was that the same damage and phase-gradient perturbations will be consistently nearly equal on the two OAM beams.

To test our hypothesis, the OAM LOS link was set with the receiving array at 50m from the transmitting OAM antenna, such that the RX linear 4-element array was approximately tangent to the bottom edge of the (up-tilted) OAM conical beams. A data stream was modulated onto the RF carrier and transmitted on beam OAM+2 with a clear LOS to the far-field receiver, which captured the signals received on all 4 antennas. Next, the same process was repeated with the modulated carrier transmitted on beam OAM+4 and receive signals were captured. Then a partial obstruction (first author on a step-ladder; see Figure 5) was positioned at 10m from the OAM antenna, in its near field, but off-axis. (Note for scale, the parking-space marking lines are $\sim 2 - 2.5$ m apart in the picture in Figure 5.) The above processes were repeated with the obstruction in place and corresponding RX signals being captured with OAM+2 and OAM+4 for comparison.

The receiving equipment was positioned in LOS in the far field at 50m from the OAM transmitter and aligned with the 1 degree cone angle of the OAM beams using a laser. It consisted of a linear array of four RHCP horn antennas, each connected to a 28 GHz receiver and coherent down-converter, which converted the signals coherently to baseband and captured them with synchronous digital-to-analog converters (DACs) on an evaluation system. The signals were post-processed in MATLAB, including maximal-ratio combining based on estimated channel-matrix pseudo-inverse. The receiving and signal-processing setup is shown in Figure 6.

The 4 elements of the receiving antenna array in Figure 6 were spaced apart by 14 cm to span an aperture no larger than that of the transmitting antenna. They were connected to receivers denoted in linear order as RX1,

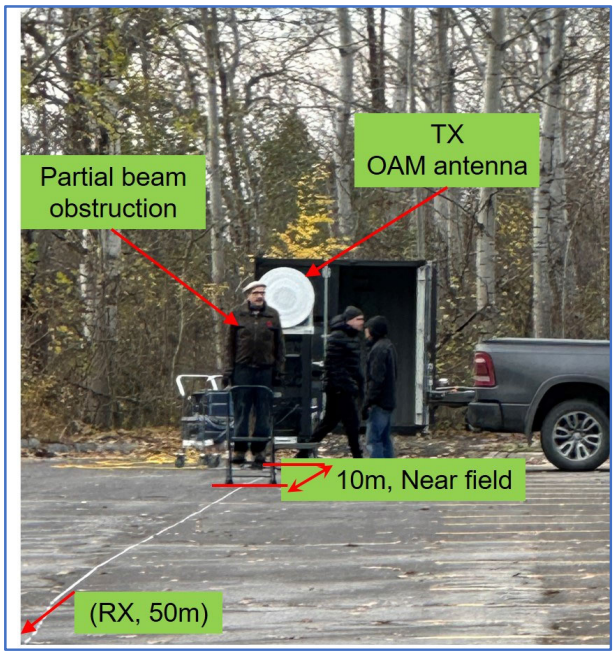

FIGURE 5. Transmitting end of 50m long experimental LOS link with partial obstruction in near field of transmitting OAM antenna.

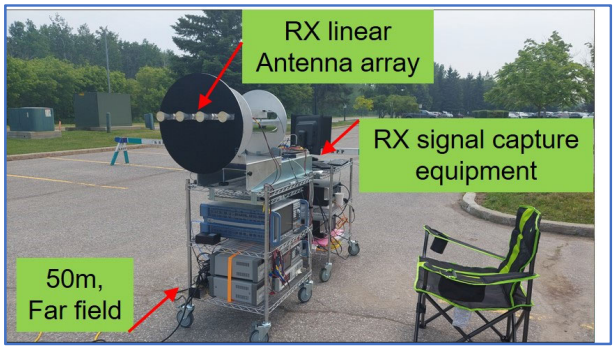

FIGURE 6. Receiving end of experimental OAM outdoor link.

RX2, RX3 and RX4; up to 4 OAM modes could be received.

Changes produced in the received signals by the same partial obstruction were characterized for each OAM mode and are summarized in Table 2 below.

It can be seen that the average signal parameters were less degraded by the same partial obstruction in OAM+4 relative to the greater degradation in OAM+2. Almost no impact on the pre-combining RX phases, and a smaller impact on the phase-gradients at the ends of the RX array, was observed on OAM+4. These findings are consistent with our hypothesis that at least partial self-healing is occurring on each OAM beam, and is more effective on the higher-order OAM+4 beam than on OAM+2 beam.

A more graphic indication of the superior self-healing in beam OAM+4 relative to that in beam OAM+2 is evident in the differences between the correlation functions of pilot

TABLE 2. Average degradations of signal parameters by partial beam obstruction in OAM+2 and OAM+4.

Signal Parameters →	RX Signal Power, dB	RX SNR, dB	RX EVM, %	Propagation Channel RX #1 #2 #3 #4 Phases, degrees	Phase Gradient RX_{12} RX_{34} degrees
Changes due to partial obstruction of beam OAM+2					
Change Averaged over 4 Receivers	-6.05	-4.5	+2.74	+97.6, +98.6, 211, +93.1	+1.1 -2.7
Changes due to partial obstruction of beam OAM+4					
Change Averaged over 4 Receivers	-1.63	-0.18	+2.26	0.0, 0.0, 0.0, 0.0	+0.3 -1.4

signals in Figure 7 and Figure 8. The same pilot signals were transmitted on each OAM beam one at a time and captured on each of the four RX antennas. They were correlated with the source pilot signal before any combining. The correlation magnitudes for the clear LOS and partially-obstructed LOS were plotted together versus time-lag in Figure 7 for beam OAM+2 and in Figure 8 for beam OAM+4.

The pilot signal in each case was a pseudo-BPSK (pseudo-random symbols {(1+j), (-1-j)} at 30.72 Msymbols/s) signal sampled at 122.88 Msamples/s.

By inspection of Figures 7 and 8, it is clear that the degradations of the pilot correlations with the pilot signals received on beam OAM+2 caused by the partial obstruction, were greater than the corresponding degradations observed on beam OAM+4, caused by the same obstruction. Although the self-healing is never complete [5], some impact of the propagation channel does occur on both OAM beams. The observed fact that there is less impact on the higher-order OAM beam than on the lower-order one, indicates that self-healing is taking place in accordance with our hypothesis.

Because the beam-widths of both OAM beams were arranged to be equal and the signal strengths at the RX site were also adjusted to be equal, the differences in the propagation channels were dominated by the phase structures of the OAM beams. Consequently, these differences were the chief causes of the different degrees of self-healing effected by the phase structures of the OAM beams, when they experienced the same partial obstruction. This is evidenced by the greater residual effect observed in the pilot correlations on beam OAM+2 as compared to that observed on beam OAM+4.

Equivalently, in the presence of antenna site constraints, migrating a MIMO data transmission in a case of partial antenna obstruction from beam OAM+2 to beam OAM+4 provides some noticeable degree of self-healing from the effects of the obstruction. This improves the quality of the spatial channel and recovered data. This finding supports our initial hypothesis based on the relevant literature.

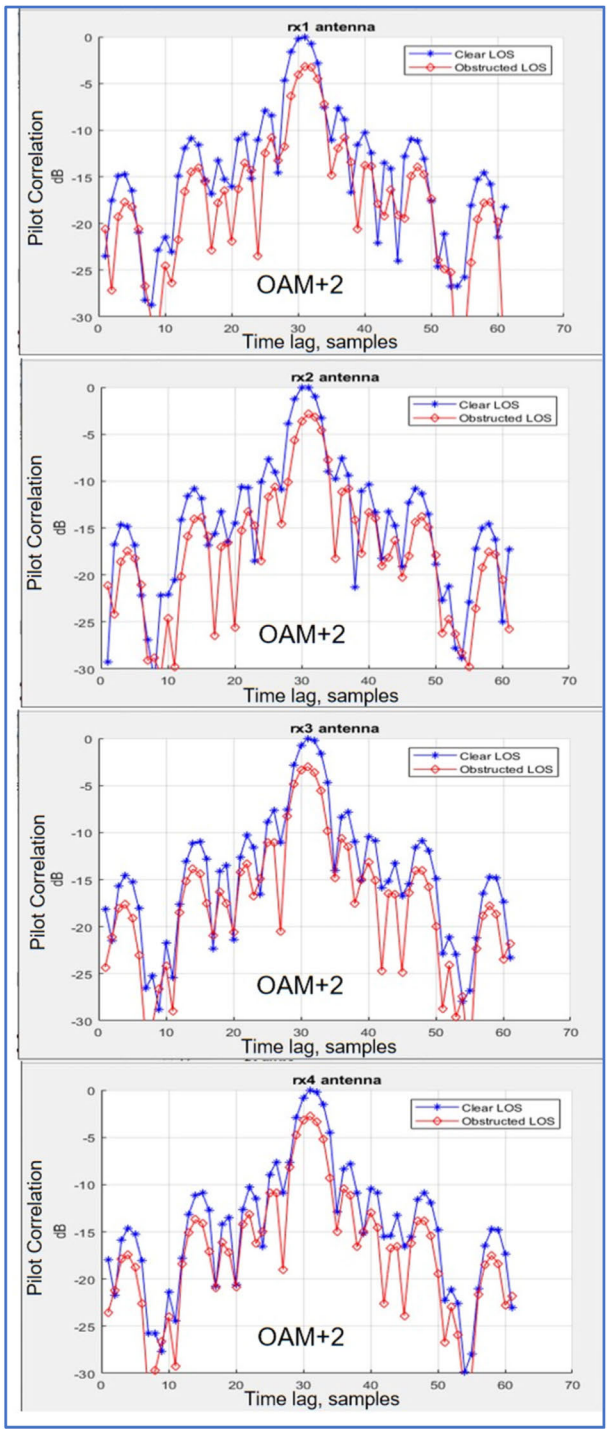

FIGURE 7. Effects of partial obstruction of beam OAM+2 on the correlations of pilot signals received on each RX antenna.

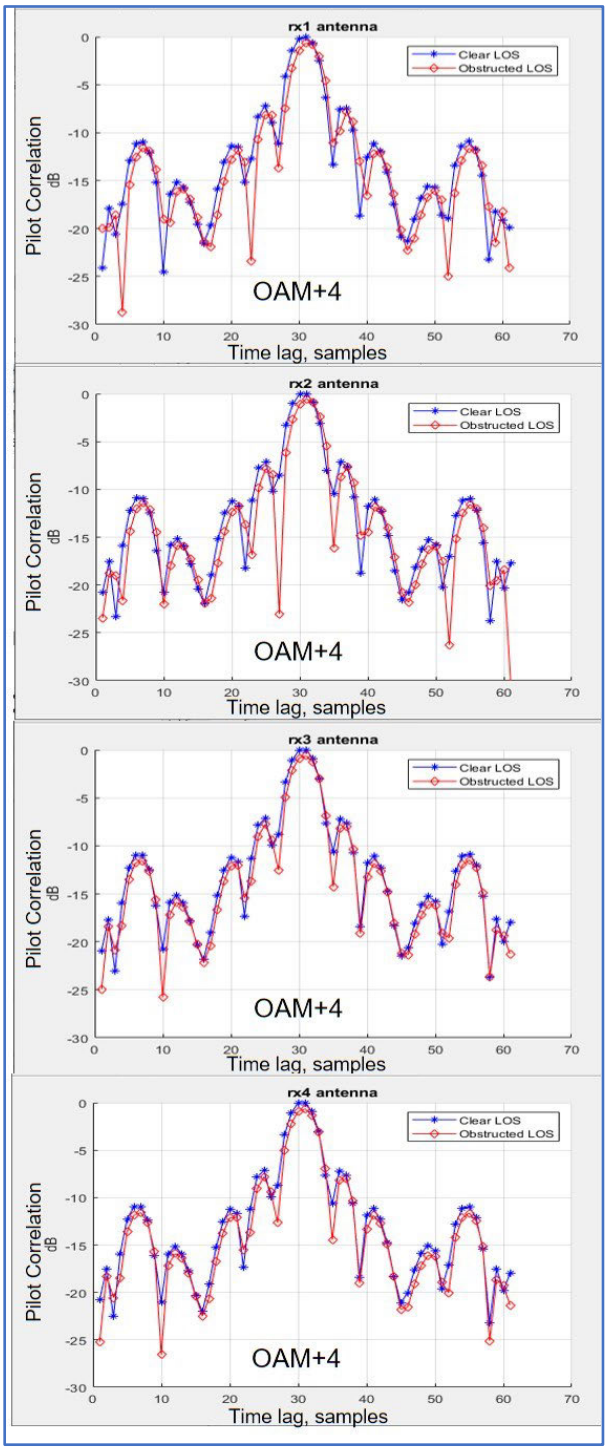

FIGURE 8. Effects of partial obstruction of beam OAM+4 on the correlations of pilot signals received on each RX antenna.

IV. A PHYSICAL MODEL OF OAM SELF-HEALING

Recall from Section I that the equi-phase contours of an OAM beam form spirals around the beam z-axis. The Poynting vector is then locally orthogonal to these phase-fronts and also forms spirals around the beam z-axis, as shown in Figure 9. The free-space wavelength is associated with the wave vector $k = 2\pi/\lambda = 2\pi cf$, which points in the same direction as the Poynting vector.

Note that the local free-space wave vector at some location, $\{z, R\}$ is not parallel to the beam axis, but is offset in the direction tangential to the cone of the OAM beam by a vector k_T. It will shortly be shown with the help of Figure 10

and reference [8], that this tangential wave-vector and the axial wave vector along the z axis form a Pythagorean right triangle with the free-space wave-vector, k, as

$$k^2 = k_z^2 + k_T^2 \tag{2}$$

In the treatment of reference [8], an additional wave vector in the radial direction, k_r^2, is added in the right side of (2), but for simplicity, here we will ignore this component by assuming the local shape of the OAM beam at $z = L$ is cylindrical rather than conical. A portion of such local cylinder, corresponding to one 2π cycle of electrical phase, is shown unrolled at the bottom of Figure 9.

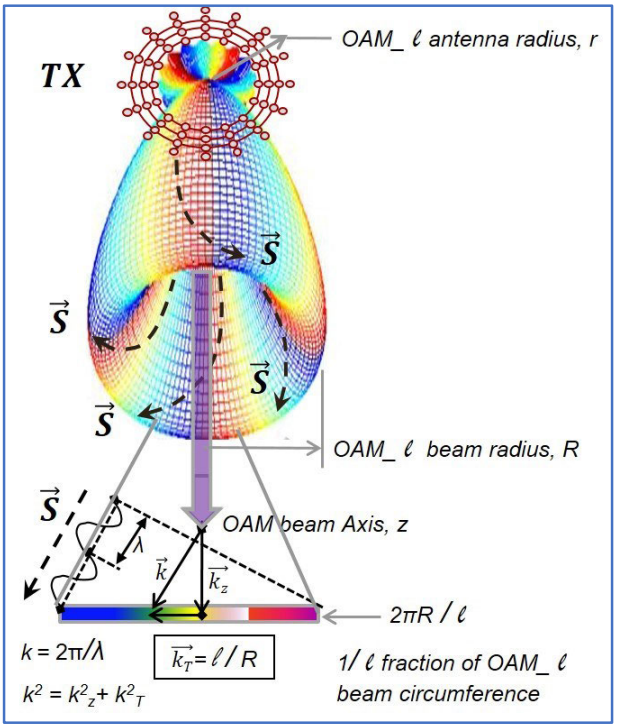

FIGURE 9. Poynting vectors and wave vectors associated with OAM beam, with simplified details in vicinity of a fixed location on beam's z-axis, where its cone has radius *R*.

It will be appreciated that the radius R increases with z as one proceeds along the beam axis into the far field, where at z=L, we have approximately $sin(\theta) \sim tan(\theta) \sim R/L$ in equation (1). Taking the peak of beam OAM_ℓ to be at approximately $x = \ell+1$ in Figure 4, leads to

$$R\,(z = L) \approx \frac{L\,(l+1)}{rk} \tag{3}$$

where r is the radius of the transmitting OAM circular antenna array (scaled to OAM+2 per Figure 4), k is the free-space wave vector and ℓ is the order of the OAM mode.

With the aid of Figure 9, one way to think about the self-healing property of OAM beams is that the Poynting vector "winds around" the partial obstruction as the OAM wave-front propagates, due to the tangential component of the wave vector, k_T. Note that the wave vectors relate to phase velocities in their respective directions. As the beam propagates, this tangential wave vector k_T moves the phase-fronts around the periphery of the conical main lobe of the OAM beam. The partial obstruction interrupts this tangential progression by blocking some of the phase-fronts, but the successive ones that are not blocked, act as Huygens sources and propagate into the shadow of the partial blockage. The more phase-fronts per circumference of the OAM beam, the more successful they will be in filling the shadow region. That is intuitively one reason why higher-order OAM beams tend to self-heal better than lower-order ones.

We show next that this tangential vector responsible for the self-healing effect is directly proportional to the OAM order, and its magnitude is given by

$$k_T = \ell/R \tag{4}$$

Equation (4) then predicts that the self-healing effect is greater at smaller beam radii closer to the OAM antenna, and also increases with OAM order, ℓ, which agrees with our hypothesis. (The afore-mentioned radial component of the wave vector also contributes to filling in the shadow region in general structured beams, but was ignored for simplicity in this exposition, because the OAM beams were not deliberately structured in the radial direction, being radiated essentially from a narrow circular ring of antenna elements.)

To complete this rationale, it remains to derive the wave vectors related in equations (2) and (4) above. To that end we employ reference [8] as it relates to equations (4) - (7) therein, beginning with the cut-off OAM mode number in a coaxial waveguide carrying a radially-polarized wave. This cut-off condition can be derived with the aid of Figure 10 beginning with the familiar relation for the cut-off wavelength of the lowest-order TE mode in a rectangular waveguide. To illustrate, Figure 10 depicts the evolution of the rectangular waveguide into a coaxial waveguide, with the perfect electrical conductor (PEC) boundary condition replaced by a phase-continuity condition, and the half wavelength replaced by a full wavelength (to preserve phase-continuity modulo 2π radians). The coaxial waveguide behaviour is supported by the analysis in reference [8].

We further evolve this behaviour to radiated OAM beams, proceeding from the cylindrical structure and radial polarization in the coaxial waveguide, to the conical beam structure and arbitrary polarization of the radiating OAM beam in Figure 10.

Recall that in the rectangular waveguide, the transverse electric fields (E_y) arrange themselves so that their zero-value nodes fall on the PEC boundaries along the x-axis (x=0 and x=a) in the transverse-electric (TE) modes. This corresponds to the projection of the nodes from a plane-wave component having free-space wavelength λ propagating in the waveguide at angle α to the x-axis, as shown for

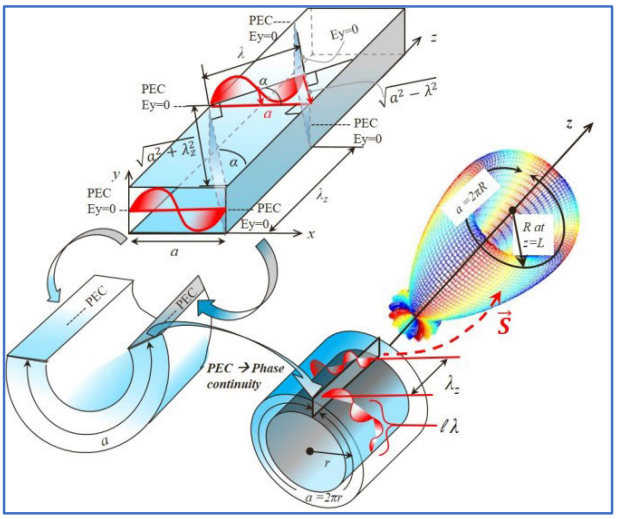

FIGURE 10. Illustration of the derivation of the wave vectors comprising a local region of an OAM beam.

one wavelength in Figure 10.

$$\cos\alpha = \frac{\lambda}{a} \tag{5}$$

$$\sin\alpha = \frac{\sqrt{a^2-\lambda^2}}{a} \tag{6}$$

$$\tan\alpha = \frac{a}{\lambda_z} = \frac{\sin\alpha}{\cos\alpha} \tag{7}$$

It also corresponds to the guided-wavelength along the z-axis, λ_z, which can be determined from the geometry using (5)-(7) above, as

$$\lambda_z = \frac{\lambda}{\sqrt{1-\left(\lambda/a\right)^2}} \tag{8}$$

We have used the projection of the zero-E_y-field at one free-space plane-wave length instead of the one at half of that wavelength because we want to preserve phase continuity in the subsequent development.

Proceeding down from the rectangular waveguide in Figure 10, we visualize bending the broad walls around the z-axis so that the short walls with the PEC boundary condition come toward each other along the circular path of the bend, as in the lower left of Figure 10. As we continue bending the waveguide, the "a" dimension forms the circumference of a circle of radius $r{=}2\pi/a$ and the PEC boundary walls merge together. Then the top broad wall becomes the inner cylindrical conductor and the bottom broad wall becomes the outer conductor of a coaxial waveguide, and the merged short walls merge the zero-field nodes of the transverse electric field with phase continuity. We can now substitute $a{=}2\pi r$ for the broad wall width, and any number of whole free-space wavelengths, $\ell\ \lambda$, for λ in equation (8) to obtain the guide wavelength for a coaxial waveguide of radius r as

$$\lambda_z = \frac{\lambda}{\sqrt{1-\left(\frac{\ell\lambda}{2\pi r}\right)^2}} \tag{9}$$

which agrees with equation (6) of reference [8] for the OAM cut-off wavelength. To see this in terms of wave vectors, we next square both sides of (9) and isolate the free-space wavelength in terms of the guide wavelength. At the same time we migrate from the coaxial waveguide to free space at $z = L$, where we have the OAM beam radius R in place of waveguide radius, r. Since R increases with z, there is no longer an OAM mode cut-off in free space. This results in

$$\lambda = \frac{\lambda_z}{\sqrt{1+\left(\frac{\ell\lambda_z}{2\pi R}\right)^2}} \tag{10}$$

which we then proceed to express in terms of wave vectors defined as $k{=}2\pi/\lambda$ and $k_z{=}2\pi/\lambda_z$.

$$k = \frac{2\pi}{\lambda} = \frac{2\pi}{\lambda_z}\sqrt{1+\left(\frac{\ell\lambda_z}{2\pi R}\right)^2} \tag{11}$$

Squaring both sides of (11) allows to rewrite it as

$$\left(\frac{2\pi}{\lambda}\right)^2 = \left(\frac{2\pi}{\lambda_z}\right)^2 + \left(\frac{\ell}{R}\right)^2 \tag{12}$$

which is recognized as equation (2) with the correspondence of the tangential wave vector as defined in equation (4). It is this tangential wave vector in equation (4) which is responsible for most of the self-healing effect observed in the relative results of the experiments described in this paper.

V. CONCLUSION AND FUTURE WORK

This paper describes, to the best of our knowledge for the first time, the effects of self-healing of OAM beams in a mm-wave experimental communications link. The effects were observed in relative terms on two different OAM beams which were arranged to be equivalent in their beam parameters except for their helical phase structures, i.e. their orders, ℓ, of OAM which was expected to be responsible for the different amounts of self-healing observed. The beams were received one at a time on a 4-antenna MIMO experimental receiver and captured for post-processing. Although the beam structures were not amenable to direct measurement as in experiments performed by prior researchers, we measured communications link and channel parameters such as SNR, EVM, channel phases from OAM transmitter to each MIMO receiver and correlations of received pilot signals with the source pilot signal. Impacts of a near-field partial obstruction of the transmitting OAM antenna were noted for OAM+2 and compared with the impacts of the same obstruction on OAM+4. The impact of partial obstruction was greater on OAM+2 than on OAM+4, indicating that more self-healing occurs on the higher-order OAM beam, which agrees with our hypothesis. A physical model of the self-healing mechanism

at work here was described, which led to the hypothesis that if self-healing was observed, it would be greater on higher-order OAM beams, and manifest as a greater impact of the partial obstruction on the lower-order OAM beam.

This physical model does not predict any quantitative effects of self-healing or obstruction, but it does agree with analyses and experiments described in prior literature, mostly in the optical field. In future work we plan to apply various MIMO combining algorithms and further characterize the robustness of multiple simultaneous OAM beams to partial obstructions.

REFERENCES

[1] M. J. Padgett, "Orbital angular momentum 25 years on [Invited]," *Opt. Exp.*, vol. 25, no. 10, p. 11265, 2017.

[2] B. Sheleg, "A matrix-fed circular array for continuous scanning," *Proc. IEEE*, vol. 56, no. 11, pp. 2016–2027, Nov. 1968.

[3] Y. Shen, S. Pidishety, I. Nape, and A. Dudley, "Self-healing of structured light: A review," *J. Opt.*, vol. 24, no. 10, Oct. 2022, Art. no. 103001.

[4] M. Klemes, A. Buliga, G. Bowles, M. Schwartzman, S. Thirakoune, T. H. Ho, D. Wessel, and W. Tong, "Multiple OAM signal recovery using Pseudo–Doppler technique with two mm-wave receivers," in *Proc. IEEE Int. Conf. Commun. Workshops (ICC Workshops)*, Jun. 2021, pp. 1–7.

[5] D. Inserra and G. Wen, "Demystifying self-healing property of accelerating beams for obstacles circumvention in communication applications," in *Proc. Photon. Electromagn. Res. Symp. (PIERS)*, Hangzhou, China, Apr. 2022, pp. 673–681.

[6] A. Aiello, G. S. Agarwal, M. Paúr, B. Stoklasa, Z. Hradil, J. Řeháček, P. de la Hoz, G. Leuchs, and L. L. Sánchez-Soto, "Unraveling beam self-healing," 2017, *arXiv:1708.00175*.

[7] S. Ramachandran and P. Kristensen, "Optical vortices in fiber," *Nanophotonics*, vol. 2, nos. 5–6, pp. 455–474, Dec. 2013.

[8] M. Pu, X. Ma, Z. Zhao, X. Li, Y. Wang, H. Gao, C. Hu, P. Gao, C. Wang, and X. Luo, "Near-field collimation of light carrying orbital angular momentum with bull's-eye-assisted plasmonic coaxial waveguides," *Sci. Rep.*, vol. 5, no. 1, Jul. 2015, Art. no. 12108, doi: 10.1038/srep12108.

MAREK KLEMES (Life Senior, IEEE) was born in Brno, Czech Republic, in April 1958. He received the B.A.Sc. (Hons.) and M.A.Sc. degrees in electrical engineering from the University of Toronto, Toronto, Canada, in 1981 and 1983, respectively, and the Ph.D. degree in electronics from Carleton University, Ottawa, Canada, in 1997. From 1983 to 1996, he was an Adaptive Systems Engineer with Canadian Marconi Company, where he developed adaptive antenna array subsystems for UHF tactical radios for U.S. Army (CECOM) and commercial wireless base-stations and super-resolution direction-finding test bench for Canadian Department of Defense (DREO). Then, he was a Senior Radio Systems Engineer with Nortel, Ottawa, from 1996 to 2001, and Dragonwave Inc., Kanata, from 2001 to 2012, involved in propagation channel modeling and link budget design, lightning protection and radio system design and testing, detailed simulation, design, integration, and prototyping of modem subsystems, such as PLLs, adaptive equalizers, AGCs, cross-polarization interference canceller (XPIC), diversity combiners, and beam-formers. Since 2012, he has been a Senior Wireless Research Engineer with Huawei Canada Research & Development Center, Kanata, working on 5G and 6G millimeter-wave waveforms and associated RF analog and adaptive subsystems and signal-processing algorithms. He holds ten patents, has published 20 articles, and enjoys all aspects of rock-hounding and antique radio experimentation. His research interests include spatial multiplexing using orbital angular momentum (OAM) waves, OAM antenna design and propagation phenomena, MIMO reception techniques, blind signal-separation (BSS) adaptive algorithms, and wireless and optical sensing techniques.

LAN HU received the M.Sc. degree from Shanghai Jiaotong University, China, and the Ph.D. degree from the University of Limerick, Ireland. From 1996 to 2009, she was with the Nortel Wireless Advanced Technologies Division. She joined Huawei Ottawa Advanced Wireless Technologies Laboratory, in 2009. As a Senior Principal Researcher in wireless technologies, she has involved many projects from 2G to 6G research and product development.

GREGORY J. BOWLES received the B.Eng. degree in electrical engineering (communications) from Canadian Royal Military College (RMC), in 1995, with a focus on computer aided design (CAD), electromagnetics, and circular polarization. He joined Nortel Networks, in 1998, where he specialized in improved corporate design techniques, CAD work flow, and high efficiency systems, including novel Doherty amplifier architectures. In 2009, he joined the Ottawa Advanced Wireless Technology Laboratory, Huawei Technologies Canada Company Ltd., with an initial focus on high efficiency power amplifier designs before migrating to transceiver and Butler matrix designs, with a particular concentration on how they apply to orbital angular momentum (OAM)-based systems.

MOHAMMAD AKBARI (Member, IEEE) received the Ph.D. degree in electrical and computer engineering from Concordia University, Montreal, QC, Canada, in 2018. He was a Postdoctoral Fellow with the University of Waterloo, Waterloo, ON, Canada, in 2019. Also, in 2020, he was a member of the Electromagnetic Vision (EMVi) Research Laboratory, McMaster University, Hamilton, ON, Canada. He joined Huawei Technologies Canada Company Ltd., Canada Research Centre, Kanata, in 2021, as a Senior Engineer. He is the author or coauthor of more than 80 peer-reviewed scientific journal articles and international conference papers. His current research interests include reconfigurable antennas, phased array antennas, metasurfaces and metamaterials, miniaturisation approaches, mutual coupling reduction techniques, feeding networks, RCS reduction, polarizers, and ultra-wideband (UWB) technology. He was a recipient of the Postdoctoral Fellowships from Fonds de Recherche du Québec—Nature et Technologies (FRQNT), in 2019, the PERSWADE/NSERC-Create Training Programme Award, in 2017, the Accelerator Award, in 2017, the Graduate Concordia Merit Scholarship, in 2016, and the Concordia University International Tuition Fee Remission, in 2014. He served as a Reviewer for the IEEE Antennas and Propagation Society's journals and magazines.

SOULIDETH THIRAKOUNE received the B.A.Sc. degree in electrical engineering from the University of Ottawa, Ottawa, ON, Canada, in 1999. From 1999 to 2011, he carried out research with the Communication Research Centre Canada, Ottawa, as a Microwave Antenna Designer on printed antennas, dielectric-resonator antennas, and holographic antennas. He joined Huawei Technologies Canada Company Ltd., Canada Research Center, Kanata, in 2012, as a mmWave Antenna Design Engineer. He is currently working on various projects involving a wide range of antennas and arrays, including novel printed antennas, multilayer microstrip antennas, microwave lenses, active integrated antennas, and waveguide antennas.

MICHAEL SCHWARTZMAN received the M.Sc. degree in mechanical engineering with experience in machine development and design, electronic packaging design, finite element analysis, and structural strength calculations, from conceptual design and prototyping to detailed design and manufacturing.

KEVIN ZHANG received the bachelor's and master's degrees in EE from BUAA. His research interests include signal processing, hardware, and FPGA design. He have worked in multiple telecom companies as a senior engineering position.

TAN HUY HO received the B.S. degree in EE from the University of Victoria, in 1996, and the M.S. degree from Carleton University, in 2014. He has been in the wireless and datacom industries for over 28 years working in companies, including start-ups and large corporations, such as Nortel, Ciena Corporation, Spirent Communications, Ericsson, and has been at Huawei Technologies Canada, since 2014. His current focus and interest with Huawei is research in mmW/sub-THz wireless system architecture and technologies, particularly, microwave-photonics technologies for 6G wireless integrated sensing and communications.

DAVID WESSEL is a graduate of the University of Wisconsin–Madison. He has been a Technical VP with Huawei Technologies Canada. He has been employed with Huawei, since 2009. Previously, he was with Nortel, from 1991 to 2009, and Microwave Modules and Devices, from 1987 to 1991.

WEN TONG (Fellow, IEEE) is currently the CTO with Huawei Wireless. He is also the Head of Huawei Wireless Research. In 2011, he was appointed as the Head of the Communications Technologies Laboratories, Huawei. He is also the Huawei 5G Chief Scientist and leads Huawei's ten year-long 5G wireless technologies research and development. Prior to joining Huawei, in 2009, he was the Nortel Fellow and the Head of the Network Technology Laboratories, Nortel. He joined the Wireless Technology Laboratories, Bell Northern Research, Canada, in 1995. He is also the Industry Recognized Leader of Invention of Advanced Wireless Technologies.

He was elected as a Huawei Fellow. He is a fellow of Canadian Academy of Engineering and Royal Society of Canada. He was a recipient of IEEE Communications Society Industry Innovation Award for "The leadership and contributions in development of 3G and 4G wireless systems," in 2014, and the IEEE Communications Society Distinguished Industry Leader Award for "Pioneering technical contributions and leadership in the mobile communications industry and innovation in 5G mobile communications technology," in 2018. He was also a recipient of R. A. Fessenden Medal. For the past three decades, he had pioneered fundamental technologies from 1G to 6G wireless and Wi-Fi with more than 520 awarded U.S. patents. He serves as the Board of Director for Wi-Fi Alliance.